08 Dec 2020

Structural Determinants of Flavin Dynamics in a Class B Monooxygenase

Ashley C. Campbell

Reeder Robinson

Didier Mena-Aguilar

Pablo Sobrado
Missouri University of Science and Technology, psobrado@mst.edu

et. al. For a complete list of authors, see https://scholarsmine.mst.edu/chem_facwork/3946

Recommended Citation

A. C. Campbell et al., "Structural Determinants of Flavin Dynamics in a Class B Monooxygenase," *Biochemistry*, vol. 59, no. 48, pp. 4609 - 4616, American Chemical Society, Dec 2020.
The definitive version is available at https://doi.org/10.1021/acs.biochem.0c00783

Biochemistry

pubs.acs.org/biochemistry Article

Structural Determinants of Flavin Dynamics in a Class B Monooxygenase

Ashley C. Campbell, Reeder Robinson, Didier Mena-Aguilar, Pablo Sobrado,* and John J. Tanner*

Cite This: *Biochemistry* 2020, 59, 4609–4616 Read Online

ACCESS | Metrics & More | Article Recommendations | Supporting Information

ABSTRACT: The ornithine hydroxylase known as SidA is a class B flavin monooxygenase that catalyzes the first step in the biosynthesis of hydroxamate-containing siderophores in *Aspergillus fumigatus*. Crystallographic studies of SidA revealed that the FAD undergoes dramatic conformational changes between *out* and *in* states during the catalytic cycle. We sought insight into the origins and purpose of flavin motion in class B monooxygenases by probing the function of Met101, a residue that contacts the pyrimidine ring of the *in* FAD. Steady-state kinetic measurements showed that the mutant variant M101A has a 25-fold lower turnover number. Pre-steady-state kinetic measurements, pH profiles, and solvent kinetic isotope effect measurements were used to isolate the microscopic step that is responsible for the reduced steady-state activity. The data are consistent with a bottleneck in the final step of the mechanism, which involves flavin dehydration and the release of hydroxy-L-ornithine and $NADP^+$. Crystal structures were determined for M101A in the resting state and complexed with $NADP^+$. The resting enzyme structure is similar to that of wild-type SidA, consistent with M101A exhibiting normal kinetics for flavin reduction by NADPH and wild-type affinity for NADPH. In contrast, the structure of the M101A–$NADP^+$ complex unexpectedly shows the FAD adopting the *out* conformation and may represent a stalled conformation that is responsible for the slow kinetics. Altogether, our data support a previous proposal that one purpose of the FAD conformational change from *in* to *out* in class B flavin monooxygenases is to eject spent $NADP^+$ in preparation for a new catalytic cycle.

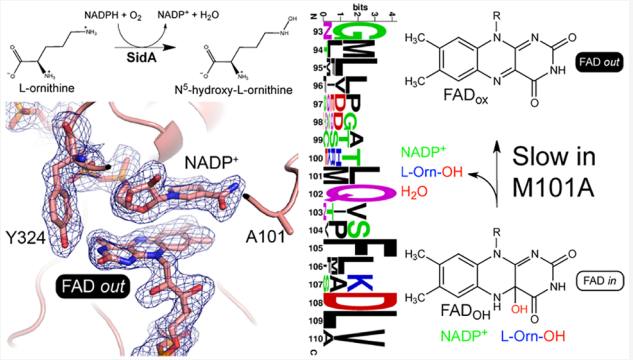

The SidA ornithine hydroxylase (UniProt E9QYP0) catalyzes the first step in the biosynthesis of hydroxamate-containing siderophores in the pathogenic fungus *Aspergillus fumigatus*.[1,2] The essential role of SidA in siderophore biosynthesis and the lack of a *sidA* gene in animals have motivated the development of inhibitors of SidA to disable the pathogen's ability to acquire iron from the host during infection.[3]

SidA is an N-hydroxylating flavin-dependent monooxygenase (NMO) that catalyzes the hydroxylation of L-ornithine (L-Orn) to N^5-hydroxy-L-Orn (Figure 1).[4,5] The multistep kinetic mechanism of SidA begins with reduction of the enzyme-bound FAD with NADPH (Figure 2). Reaction of the reduced FAD with molecular oxygen yields the C4a-hydroperoxyflavin intermediate (FAD_{OOH}). L-Orn then is hydroxylated by FAD_{OOH} to generate the product N^5-hydroxy-L-Orn and

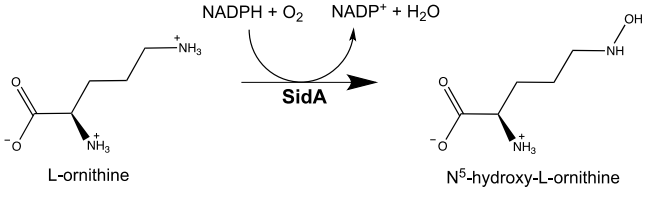

Figure 1. Reaction catalyzed by SidA.

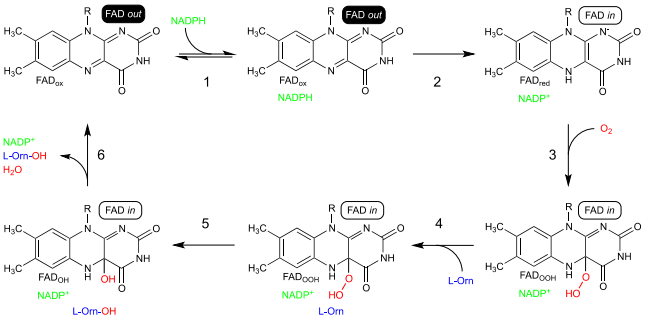

Figure 2. Kinetic mechanism of SidA. The conformation of the isoalloxazine is noted in the ovals.

Received: September 22, 2020
Revised: November 9, 2020
Published: November 23, 2020

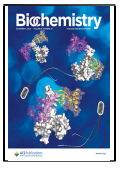

https://dx.doi.org/10.1021/acs.biochem.0c00783
Biochemistry 2020, 59, 4609–4616

C4a-hydroxyflavin. Hydrolysis of the latter and product release complete the catalytic cycle. A notable feature of the mechanism of SidA, as well as other class B flavin monooxygenases, is that $NADP^+$ remains bound to the enzyme until the final step of product release. It is thought that $NADP^+$ stabilizes the C4a-hydroperoxyflavin, preventing uncoupling of the reductive and oxidative half-reactions and the release of the reactive oxygen species, H_2O_2.[6]

Dynamics is a relatively new aspect of the mechanism of SidA and other related ornithine hydroxylases. We recently reported the first structure of the resting conformation of SidA, i.e., the state immediately before NADPH binding (Figure 3).[7]

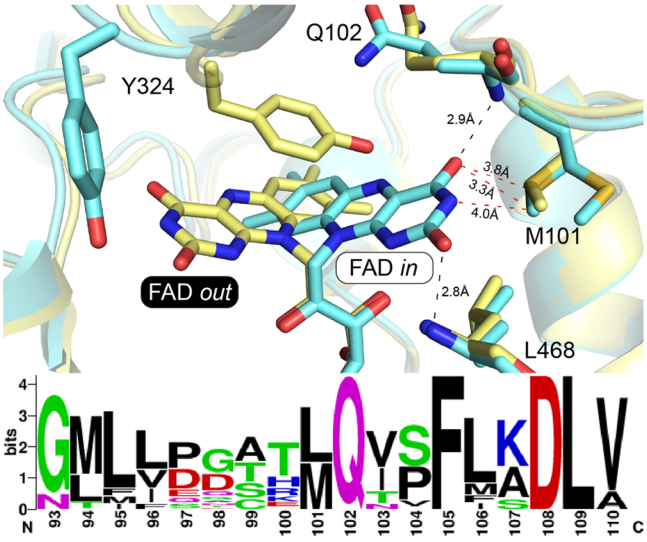

Figure 3. Comparison of the *out* and *in* conformations of wild-type SidA. Superposition of the resting conformation (yellow, PDB entry 6X0H) and SidA complexed with $NADP^+$ (aquamarine, PDB entry 6X0I). The FAD is oxidized in both structures. Met101 is the residue mutated in this study. $NADP^+$ has been omitted for the sake of clarity. Black dashes denote FAD−protein hydrogen bonds observed in the *in* state. Red dashes denote close contacts between the *in* FAD and Met101. The sequence logo was generated from 1241 sequences with WebLogo.[11]

Remarkably, the FAD isoalloxazine of the resting state is rotated out of the active site compared to other SidA structures (Figure 3). Movement between the *out* and the more typical *in* conformation involves dual dihedral rotations of 180° and 90° around the N10−C1′ and C1′−C2′ bonds of the FAD ribityl, respectively. This motion is substantial; the pyrimidine edge of the isoalloxazine moves by 9.5 Å. It is also catalytically relevant, because the active face of the isoalloxazine (*re*-face) is hidden in the *out* conformation. Movement of the FAD is accompanied by a 10 Å conformational change of the Tyr loop. In the *out* conformation, the eponymous residue of the Tyr loop stacks against the *si*-face of the FAD. Either the binding of NADP(H) or reduction of the FAD was sufficient to promote the *in* conformation. A similar *out* FAD conformation and movement of the Tyr loop were also observed in crystal structures of the ornithine hydroxylase KtzI (34% identical to SidA).[8] The observation of the same conformational changes in the two enzymes suggests it may be a conserved dynamic feature of ornithine hydroxylases. Although the precise role of the *out* conformation in catalysis remains to be determined, we suggested that the transfer of hydride from NADPH to the FAD occurs with the latter in an *out* conformation, and that the concerted dynamics of the FAD and protein allows $NADP^+$ to adopt the conformation needed to stabilize C4a-hydroperoxyflavin and prevent uncoupling.[7,9,10]

Here, we show that an active site methionine residue of SidA (Met101) is both a key determinant of the FAD conformation and essential for efficient catalysis. Met101 contacts the pyrimidine edge of the isoalloxazine in the *in* state and is present in approximately half of 1241 homologous sequences analyzed, including KtzI (Figure 3). The other homologues contain Leu at this position; PvdA is example of this group. The contacts formed by Met101 may help align the isoalloxazine to form hydrogen bonds with the main chain (Figure 3). We note these hydrogen bonds are also formed by PvdA, suggesting that Met and Leu at this position in the chain could have similar roles in stabilizing the *in* state. Crystal structures of SidA variant M101A show that the FAD is locked in the *out* conformation. Unlike the wild-type enzyme, the binding of $NADP^+$ to M101A fails to promote the *in* FAD conformation. Surprisingly, movement of the Tyr loop is not impaired in M101A, suggesting that the mutation decoupled the dynamics of the FAD from that of the protein. Replacement of M101 with Ala does not affect the binding of NADPH or the hydride transfer step, which is the rate-limiting step in SidA. Instead, the mutation slows a step after or at the same time as flavin oxidation, a step that most likely involves the release of $NADP^+$. These results provide insight into the origins and purpose of active site dynamics in class B flavin monooxygenases.

MATERIALS AND METHODS

Materials. *Escherichia coli* BL21(DE3)-Turbo chemically competent cells, buffers, and media were obtained from Fisher Scientific (Pittsburgh, PA). NADPH was obtained from Sigma-Aldrich (St. Louis, MO), and *E. coli* TOP-10 chemically competent cells from Invitrogen (Carlsbad, CA). Chromatography columns used for protein purification were from GE Healthcare. DNA primers were synthesized by Integrated DNA Technologies (Coralville, IA). Plasmid preparation kits were obtained from Qiagen (Valencia, CA).

Site-Directed Mutagenesis and Protein Production. The M101A variant of the SidA construct was generated from the wild-type SidA gene in pET15b. This mutation was chosen as Met101 is in the proximity of the pyrimidine edge of the isoalloxazine of SidA when the flavin is in the *in* position (Figure 3). Site-directed mutagenesis was performed using the QuikChange system (Agilent Technologies) following the manufacturer's instructions. For the mutagenesis reaction, the forward primer (5′-CGGTATGCTGGTCCCGGGCT-CGAAGGCGCAGATCAGCTTCATCAAGGATCTC-3′) and reverse primer (5′-GAGATCCTTGATGAAGCTGA-TCTGCGCCTTCGAGCCCGGGACCAGCATACCG-3′) were used. The mutated gene was sequenced to ensure that the mutation was incorporated. SidA M101A was expressed with an N-terminal His tag followed by a thrombin cleavage site.

SidA M101A was expressed in *E. coli* and purified using previously described methods.[10] In brief, the protein was expressed in BL21(DE3)-Turbo cells overnight at 25 °C. The cells were harvested by centrifugation and lysed by sonication in a buffer containing 25 mM HEPES (pH 7.5), 300 mM NaCl, 25 mM imidazole, 60 μg/mL lysozyme, 20 μg/mL DNase I, 20 μg/mL RNase, 34.2 mg of PMSF, and 150 μM FAD. The lysate was centrifuged at 45000*g* for 45 min at 4 °C.

https://dx.doi.org/10.1021/acs.biochem.0c00783
Biochemistry 2020, 59, 4609−4616

The protein was purified over two 5 mL Ni-NTA columns connected in tandem, washed with 30 mM imidazole, and eluted with 300 mM imidazole. The His tag was cleaved using thrombin as described previously.[10] Briefly, thrombin (2 mg/mL) was added to the purified protein and dialyzed into a buffer containing 25 mM HEPES (pH 7.5) and 300 mM NaCl, and thrombin (2 mg/mL) was added and incubated overnight at 4 °C. Cleaved SidA M101A for crystallization was dialyzed into a storage buffer containing 25 mM HEPES (pH 7.5) and 100 mM NaCl, flash-frozen in liquid nitrogen, and stored at −80 °C.

Determination of the Flavin Extinction Coefficient and Incorporation. The spectra of purified M101A were recorded in 100 mM sodium phosphate (pH 7.5). The bound flavin was removed by incubating the enzyme in 9% (w/v) SDS at 25 °C for 20 min. After centrifugation, the free flavin spectra were recorded. The extinction coefficient for M101A was calculated to be 10600 M^{-1} cm^{-1} at 458 nm, using an extinction coefficient at 450 nm for free FAD of 11300 M^{-1} cm^{-1}.[12] Flavin incorporation was determined by measuring the protein concentration via the Bradford assay (Bio-Rad) and comparing it to the protein concentration based on the flavin absorbance. Flavin incorporation was generally close to ∼70% for M101A, which is similar to that of wild-type SidA.[12]

Steady-State Kinetics. The rate of oxygen consumption was measured using a Hansatech (Norfolk, England) Oxygraph system. The assay solution contained 1 mL of 100 mM sodium phosphate (pH 7.5) at 25 °C. The NADPH concentration was kept constant at 1 mM, while the L-Orn concentration was varied between 0.1 and 15 mM. The assays were initiated by addition of 5 μM M101A. Reactions were monitored for 5 min with constant stirring. Hydroxylated L-Orn was measured using a variation of the Csaky iodine oxidation assay.[12,13] The standard assay buffer contained 104 μL of 100 mM sodium phosphate (pH 7.5) with varying concentrations of L-Orn and the NADPH concentration held constant at 1 mM. Reactions were initiated by addition of 5 μM M101A. Reaction mixtures were incubated for 10 min at 25 °C while being constantly shaken at 750 rpm.

Pre-Steady-State Kinetics. All rapid reaction experiments were carried out at 25 °C using an SX-20 stopped-flow spectrophotometer (Applied Photophysics, Leatherhead, U.K.) housed in an anaerobic glovebox (Coy, Grass Lake, MI). Preparation of anaerobic buffer involved five cycles of 5 min of vacuum and 1 min of flushing with O_2-free argon for 30 min total. The enzyme was made anaerobic by applying 1 min cycles of vacuum and 15 s of flushing with O_2-free argon for 5 min total. Substrates were made anaerobic by being dissolved in anaerobic buffer inside the glovebox. The stopped-flow was made anaerobic by flushing with 1 mL of anaerobic 100 mM sodium acetate (pH 5.0) containing 100 mM D-glucose and 100 μg/mL glucose oxidase Type-X. The rate of flavin reduction of M101A was measured in single mixing mode where the anaerobic enzyme (15 μM after mixing) was mixed with an equal volume of NADPH (15−500 μM after mixing).

The rate of flavin oxidation was measured in double mixing mode. Anaerobic M101A (60 μM before mixing) was first mixed with an equal volume of NADPH (60 μM before mixing). This mixture was incubated in an aging loop for 60 s until the bound flavin was fully reduced. The reduced M101A−$NADP^+$ complex was then reacted with O_2 (300 μM after mixing). Flavin oxidation was also performed in the presence of 10 mM L-Orn. Spectra were recorded on a logarithmic time scale until full reduction or oxidation was completed.

pH Dependence of Flavin Oxidation. The pH dependence of flavin oxidation was measured in double mixing mode. Anaerobic M101A (60 μM before mixing) was first mixed with an equal volume of NADPH (60 μM before mixing) in 20 mM Tris-HCl and 200 mM NaCl (pH 8.0). This mixture was allowed to incubate in an aging loop for 60 s until the bound flavin was fully reduced. The reduced M101A−$NADP^+$ complex was then allowed to react with air-saturated buffer. This air-saturated solution contained 200 mM buffer that rapidly increased the pH to the desired value in the flow cell. Between pH values of 6 and 8, sodium phosphate was used; between pH values of 8.5 and 9.0, Tris-SO_4 was used, and between pH values of 9.5 and 10.5, sodium carbonate/bicarbonate was used.

Solvent Kinetic Isotope Effect Studies on Flavin Oxidation. Solvent kinetic isotope effect (SKIE) experiments were performed in the presence and absence of 15 mM L-Orn. For the reactions in D_2O, M101A was concentrated to ∼400 μM (based on flavin content) and diluted to 60 μM in a 100% D_2O buffer of 20 mM Tris-HCl and 200 mM NaCl (pD 8.0). This gave a concentration of ∼85% D_2O, and after two mixes in the stopped-flow with 100% D_2O buffer, a final D_2O concentration of ∼96% was achieved. SKIEs in the absence and presence of L-Orn were determined at pL values of 7.0 and 9.0, respectively (pL refers to the pH or pD of the solution, and pD is equal to the pH value + 0.4, which is the variation from the change in the equilibrium on a hydrogen selective glass electrode).[14] All solutions were checked for their proper pL values with a Fisher Scientific Accumet AB15+ Basic pH meter. Spectra were recorded on a logarithmic time scale until oxidation was complete.

Data Analysis. All data were fit using KaleidaGraph (Synergy Software, Reading, PA). The rates of flavin reduction were determined by fitting the decrease in absorbance at 458 nm to a double-exponential decay equation (eq 1).

$$v = c + a_1 e^{-k_1 t} + a_2 e^{-k_2 t} \quad (1)$$

For flavin oxidation studies, the increase in absorbance at 458 nm, which corresponds to flavin oxidation by H_2O elimination in the presence of L-Orn, was fit to a triple-exponential rise function (eq 2). In the absence of L-Orn, a double-exponential function was sufficient to model the data (eq 2 with the third term omitted). The oxidation rate constant measured at 458 nm as a function of pH was fit to eq 3. This equation describes a curve with a single pK_a with increasing activity as the pH increases and plateau regions at high and low pH. C and A in eq 3 represent the upper and lower limits for the pL profile, respectively.

$$v = c + a_1(1 - e^{-k_1 t}) + a_2(1 - e^{-k_2 t}) + a_3(1 - e^{-k_3 t}) \quad (2)$$

$$y = \frac{C + A(10^{pK_a - pL})}{1 + 10^{pK_a - pL}} \quad (3)$$

Crystallization, X-ray Diffraction Data Collection, and Refinement. M101A was crystallized using conditions similar to those described for wild-type SidA.[7] Crystallization was performed in sitting drops at 293 K with an enzyme stock solution containing 8−10 mg/mL M101A in 25 mM HEPES (pH 7.5) and 100 mM NaCl. The crystallization reservoir

https://dx.doi.org/10.1021/acs.biochem.0c00783
Biochemistry 2020, 59, 4609−4616

contained 17−21% (w/v) PEG 3350, 0.1 M HEPES (pH 7.5), and 0.1 M calcium acetate. The drops were formed by mixing a 2:1 enzyme/reservoir solution. For crystallization of the $NADP^+$ complex, the enzyme stock solution contained 1 mM $NADP^+$. The crystals were cryoprotected in 15% (v/v) PEG 200, 20% (w/v) PEG 3350, 0.1 M HEPES, (pH 7.5), and 0.1 M calcium acetate.

X-ray diffraction data were collected in shutterless mode at ALS beamline 4.2.2. The data sets were integrated and scaled with XDS.[15] Intensities were converted to amplitudes with AIMLESS.[16] The space group is $P2_1$ with the unit cell dimensions listed in Table 1. The asymmetric unit contains one SidA tetramer. We note this is the same crystal form that we used previously to determine structures of wild-type SidA.[17] Data processing statistics are summarized in Table 1 and listed in detail in Table S1.

Table 1. Summary of X-ray Diffraction Data Collection and Refinement Statistics

	ligand-free	$NADP^+$
resolution (Å)[a]	61.4−2.20 (2.24−2.20)	62.9−2.10 (2.14−2.10)
mean I/σ[a]	10.8 (0.9)	9.4 (1.7)
$CC_{1/2}$[a]	0.995 (0.484)	0.993 (0.740)
completeness (%)[a]	98.7 (89.2)	96.6 (95.9)
multiplicity[a]	3.5 (2.8)	3.5 (2.9)
R_{cryst}[a]	0.194 (0.334)	0.204 (0.205)
R_{free}[a,b]	0.230 (0.378)	0.241 (0.255)
Clashscore (PR)[c]	3.38 (99)	2.94 (99)
MolProbity score (PR)[c]	1.53 (98)	1.25 (100)
average B (Å^2)		
protein	35.1	28.8
FAD	27.5	23.4
$NADP^+$	N/A	25.5
water	30.1	26.1
PDB entry	7JVK	7JVL

[a]Values for the outer resolution shell of data are given in parentheses. [b]A 2% test set. [c]From MolProbity. The percentile ranks (PR) for Clashscore and MolProbity score are given in parentheses.

PHENIX[18] was used for refinement, and Coot[19] was used for model building. The starting model for refinement was derived from the coordinates of wild-type SidA (PDB entry 6X0H for ligand-free M101A and PDB entry 6X0I for the $NADP^+$ complex). Noncrystallographic symmetry restraints were used during refinement. The structures were validated using MolProbity[20] and the wwPDB validation server.[21] Polder maps were used to validate the modeling of ligands and the Tyr loop.[22] Refinement statistics are summarized in Table 1 and listed in detail in Table S1.

RESULTS

Ultraviolet−Visible (UV−vis) Flavin Spectra of M101A. The flavin spectra for M101A show some minor changes in the λ_{max} from 450 nm for wild-type SidA (SidA henceforth) to 458 nm for M101A (Figure S1). Also, the extinction coefficient was decreased to 10600 M^{-1} cm^{-1}, compared to a value of 13700 M^{-1} cm^{-1} for SidA.

Steady-State Oxygen Consumption. The steady-state kinetic parameters for oxygen consumption for M101A were determined using L-Orn as the variable substrate and NADPH at a saturating concentration. M101A displayed reduced activity, its k_{cat} value being ∼25-fold lower than that of SidA (Table 2). The K_m value for L-Orn appears to be unaffected, indicating that mutation of Met101 does not affect the binding of L-Orn.

Table 2. Steady-State Kinetic Parameters[a]

Oxygen Consumption		
	SidA[b]	M101A
k_{cat} (s^{-1})	0.59 ± 0.01	0.023 ± 0.002
$K_{m\ (L\text{-}Orn)}$ (mM)	1.1 ± 0.3	0.7 ± 0.2
$k_{cat}/K_{m\ (L\text{-}Orn)}$ (M^{-1} s^{-1})	500 ± 100	30 ± 10
L-Orn Hydroxylation		
	SidA[b]	M101A
k_{cat} (s^{-1})	0.62 ± 0.02	0.024 ± 0.001
$K_{m\ (L\text{-}Orn)}$ (mM)	1.0 ± 0.2	1.8 ± 0.3
$k_{cat}/K_{m\ (L\text{-}Orn)}$ (M^{-1} s^{-1})	600 ± 100	14 ± 2

[a]Conditions: 100 mM sodium phosphate, pH 7.5, and 25 °C. The uncertainties were calculated from three trials. [b]Data from ref 24.

Steady-State L-Orn Hydroxylation. The steady-state kinetic parameters for L-Orn hydroxylation for M101A were calculated under saturating concentrations of NADPH. The data indicate that M101A has very similar k_{cat} values for L-Orn hydroxylation and oxygen consumption; thus, the coupling of the oxidative and reductive half-reaction is ∼100% and similar to that of SidA (Table 2 and Figure S2).

Pre-Steady-State Kinetics of Flavin Reduction and Oxidation. The rate constant for flavin reduction was measured for M101A at varying concentrations of NADPH to determine if this mutation affected the affinity for NADPH or the hydride transfer step. M101A is reduced by NADPH in a double-exponential manner similar to that of SidA (Figure S3A).[23,24] M101A is fully reduced by NADPH, and the rate constant for flavin reduction is only slightly different from that of SidA (Table 3). Although under conditions tested the K_D value could not be calculated, the fact that the maximum rate of flavin reduction was observed at 15 μM NADPH (Figure S3B) indicates that the mutation did not substantially change the K_D value for NADPH. Thus, the M101A mutation did not significantly affect the rate of reduction or affinity for NADPH.

The oxidative half-reaction in the presence and absence of L-Orn was performed to determine if the reaction with molecular oxygen, stabilization of the C4a-hydroperoxyflavin intermediate, or flavin dehydration step was affected by the mutation. Table 3 shows the rate constant for formation of the C4a-hydroperoxyflavin (k_{OOH}, step 3 in Figure 2). Similar to SidA, the reaction is enhanced when L-Orn is present for M101A. The rate constants for hydrogen peroxide release ($k_{H_2O_2}$), which occurs in the absence of L-Orn, show that elimination of hydrogen peroxide is ∼2-fold slower for M101A. In the presence of L-Orn, hydroxylation occurs and the changes in flavin spectra at 458 nm report on the dehydration of the flavin (k_{H_2O}, step 6 in Figure 2). The mutation of Met101 causes an ∼14-fold decrease in k_{H_2O} (Table 3).

pH Profile for Flavin Oxidation in the Presence and Absence of L-Orn. The pH profiles of flavin oxidation for M101A were measured to determine if this mutation changed the pK_a value for N5 of the flavin (Table 4 and Figures S4−S6). The results show similar pK_a values as calculated for SidA in the absence or presence of L-Orn, suggesting that Met101

https://dx.doi.org/10.1021/acs.biochem.0c00783
Biochemistry 2020, 59, 4609−4616

Table 3. Pre-Steady-State Kinetic Parameters for Flavin Reduction and Oxidation[a]

	Reduction		
	k_{red1} (s^{-1})	k_{red2} (s^{-1})	K_D (μM)
SidA[b]	0.62 ± 0.01	0.220 ± 0.005	~1
M101A	0.87 ± 0.01	0.25 ± 0.04	N/D

	Oxidation			
	(−) L-Orn		(+) L-Orn	
	k_{OOH} (s^{-1})	$k_{H_2O_2}$ (s^{-1})	k_{OOH} (s^{-1})	k_{H_2O} (s^{-1})
SidA[b]	0.65 ± 0.06	0.0150 ± 0.0005	18 ± 2	1.20 ± 0.03
M101A	0.73 ± 0.08	0.0080 ± 0.0001	25 ± 2	0.084 ± 0.007

[a]Conditions: 100 mM sodium phosphate, pH 7.5, and 25 °C. The uncertainties were calculated from three technical replicates. [b]Data from ref 24.

Table 4. pK_a and Solvent Kinetic Isotope Effect Values

	(−) L-Orn	(+) L-Orn
	SidA[a]	
pK_a, H_2O	>9	6.7 ± 0.1
pK_a, D_2O	>10	7.18 ± 0.05
SKIE	2.30 ± 0.07	1.59 ± 0.01
	M101A	
pK_a, H_2O	>9	6.9 ± 0.1
SKIE	1.59 ± 0.09	1.35 ± 0.08

[a]Data from ref 24. The reported uncertainties are from the fitting analysis.

does not play a major role in regulating the pK_a value of residues in the active site or the flavin N5 atom.

Solvent Kinetic Isotope Effect. The SKIEs of flavin oxidation were measured for M101A to determine if its atypical oxidation kinetics are due to a chemical step becoming more rate-limiting due to the mutation. Previously, we have shown that the SKIEs for flavin oxidation in SidA for both hydrogen peroxide and water elimination involve a proton transfer originating from N5 of the flavin.[9] The data indicate that in the absence of L-Orn, the SKIE is lower for M101A, while in the presence of L-Orn, the SKIE is only slightly lower or perhaps unchanged (see Table 4 and Figure S7). This suggests that for M101A, the much slower acceleration of flavin oxidation when L-Orn is present is not due to water elimination becoming more rate-limiting.

Structures of M101A. The crystal structure of M101A with the FAD oxidized and no substrates bound (resting state) was determined at 2.2 Å resolution. Electron density clearly indicated that the FAD was in the *out* conformation, which is expected for the resting enzyme (Figure 4A). The Tyr loop adopts the conformation associated with the *out* FAD, in which Tyr324 stacks against the *si*-face of the isoalloxazine. These observations were consistent for all four protomers of the tetramer in the asymmetric unit. The root-mean-square deviation between the resting conformations and M101A and wild-type SidA is only 0.18−0.35 Å/chain. These results suggest that the mutation did not perturb the resting structure of SidA.

The structure of M101A complexed with $NADP^+$ (FAD oxidized) was determined at 2.1 Å resolution. The electron density clearly indicated the conformations of the FAD, $NADP^+$, and Tyr324 (Figure 5A). Unexpectedly, the FAD adopts the *out* conformation despite the presence of $NADP^+$ in the active site. Although the FAD remains *out*, the Tyr loop has moved to the conformation associated with the *in* FAD (Figure 5B). Movement of the Tyr loop is necessary to avoid a steric

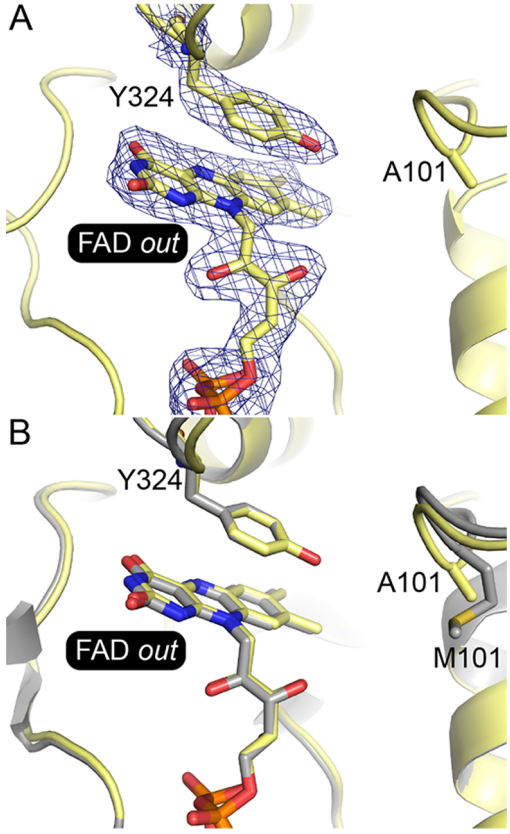

Figure 4. Structure of the resting state of M101A. (A) Electron density for the FAD and Tyr324. The mesh represents a polder omit map (3σ). (B) Comparison of the resting conformations of M101A (yellow) and wild-type SidA (gray, PDB entry 6X0H).

clash with $NADP^+$. The conformation of $NADP^+$ is identical to that of the wild-type enzyme; however, because the FAD is *out*, the $NADP^+$ packs against the *si*-face of the isoalloxazine in M101A, rather than the *re*-face as observed in the wild-type enzyme (Figure 5B).

The active site of the M101A−$NADP^+$ complex resembles the dead-end inhibited complex of wild-type KtzI (PDB entry 4TLZ), also a class B ornithine hydroxylase (34% identical to SidA).[8] In both structures, the FAD is *out*, $NADP^+$ is in the standard conformation, and the Tyr loop adopts the conformation associated with the *in* FAD (Figure 5C).

DISCUSSION

Flavin-dependent monooxygenases represent a large family of enzymes with diverse chemical activities.[6,25] The mechanism

https://dx.doi.org/10.1021/acs.biochem.0c00783
Biochemistry 2020, 59, 4609−4616

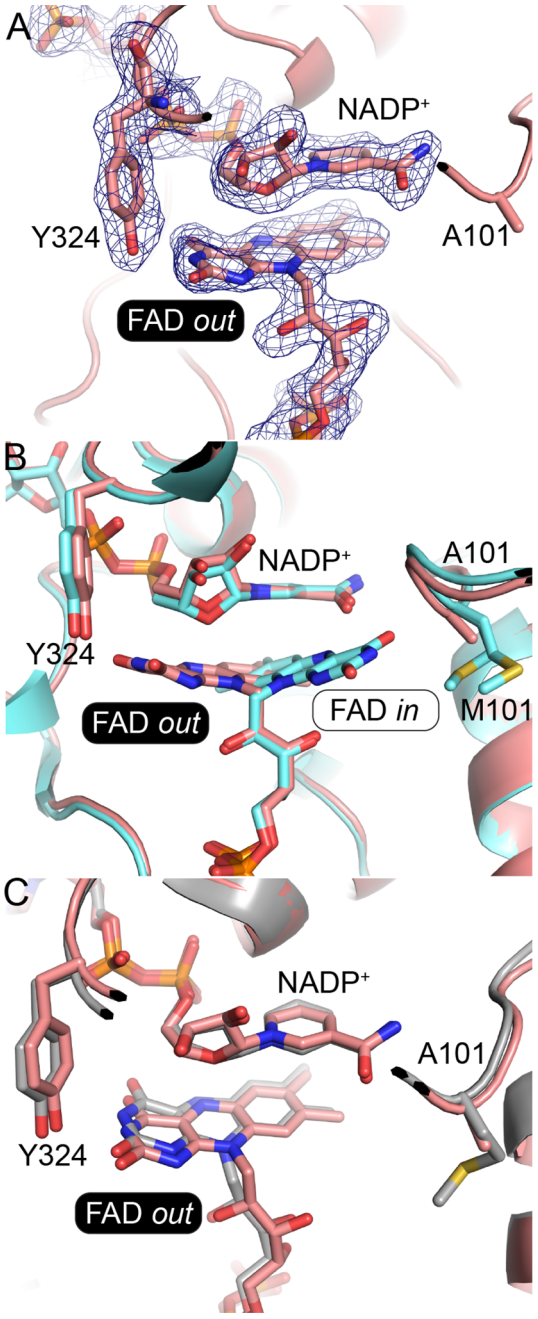

Figure 5. Structure of M101A complexed with $NADP^+$. (A) Electron density for FAD, $NADP^+$, and Tyr324 (polder omit, 3σ). (B) Comparison of the $NADP^+$ complexes of M101A (salmon) and wild-type SidA (aquamarine, PDB entry 6X0I). (C) Comparison of the $NADP^+$ complexes of M101A (salmon) and wild-type KtzI (gray, PDB entry 4TLZ).

by which these enzymes regulate the reactivity of the flavin cofactor has been the subject of intense investigation for several decades. As a result, many important aspects are currently known. For example, members of the class A flavin monooxygenase are single-component systems that contain a tightly bound FAD. In the substrate-free form, the FAD is buried, and substrate binding triggers a conformational change that exposes the isoalloxazine ring to the surface of the protein where NADPH can interact and transfer a hydride equivalent. This is known as the swinging flavin.[26] This type of mechanism used by class A monooxygenases has been coined "cautious" because reaction with NADPH occurs only when the substrate is ready for hydroxylation in the active site, which ensures coupling of the reactions.[6,25,26] Class B monooxygenases contain two Rossmann folds, one each for flavin and NADPH binding. These enzymes use a "bold mechanism", where the enzyme is reduced by NADPH, in the absence of a substrate. Furthermore, $NADP^+$ remains bound to the enzyme to stabilize the C4a-hydroperoxyflavin until a suitable substrate binds.[6]

The structures of SidA and PvdA with L-Orn bound in the active site provided the first view of how class B monooxygenases organize a flavin, NADP(H), and L-Orn for catalysis.[10,27] Mechanistic and computational analysis with SidA showed that interactions of the amide oxygen of NADP(H) with the flavin N5 atom were key in the stabilization of the C4-hydroperoxyflavin.[9,28,29] Recent work on SidA[7] and a related enzyme, KztI,[8] revealed unprecedented flavin motion in members of the class B monooxygenase family. In both enzymes, the FAD adopts an *out* conformation in the ligand-free oxidized state, which differs substantially from the *in* conformation adopted during catalysis (Figure 3).

Here, we sought insight into the origins of flavin motion in class B monooxygenases by probing the function of Met101, a residue that contacts the pyrimidine ring of the *in* FAD. Steady-state kinetic analysis of M101A shows that the activity is significantly impaired. The reduction of activity does not originate from decreased reactivity with NADPH, as the rate constants for flavin reduction were not significantly affected (Table 3). These results are consistent with the structure of the resting M101A being nearly identical to that of the wild-type enzyme.

Our data suggest that the catalytic defect of M101A originates in events occurring after flavin reduction, in the oxidative half-reaction. It has been previously shown that the pK_a of the flavin N5 atom in SidA is modulated to stabilize the C4a-hydroperoxyflavin or to facilitate flavin oxidation.[24] We determined the pK_a values for M101A in the absence of L-Orn, which represents flavin oxidation by H_2O_2 release, and in the presence of L-Orn, which reports on flavin oxidation by dehydration (Figure 2, step 6). The results show no significant changes in the pK_a values upon mutation of Met101. To determine if the chemical steps involved in flavin oxidation were affected, we performed SKIE experiments. The SKIE values were lower for H_2O_2 release (in the absence of L-Orn) and marginally lower for flavin dehydration (in the presence of L-Orn). Thus, a step that occurs at the same time or after these chemical steps is the slow step in the reaction for M101A.

We suggest that our kinetic and structural data are consistent with the mutation of Met101 affecting $NADP^+$ release. Kinetic data implicate a bottleneck in step 6 of Figure 2, which involves flavin dehydration and the release of N^5-hydroxy-L-Orn and $NADP^+$. The structure of ligand-free M101A is very similar to that of wild-type SidA, consistent with M101A exhibiting wild-type affinity for NADPH and normal flavin reduction kinetics. In contrast, the structure of the M101A–$NADP^+$ complex unexpectedly shows the FAD in the *out* conformation. This complex may represent a stalled conformation that leads to the slow kinetics observed for M101A. This interpretation is in agreement with the proposal of Setser et al. that the purpose of the FAD conformational change from *in* to *out* is to eject $NADP^+$ in the last step of catalysis.[8]

The M101A–$NADP^+$ complex perhaps represents a dead-end state that is avoided by the wild-type enzyme but is made

https://dx.doi.org/10.1021/acs.biochem.0c00783
Biochemistry 2020, 59, 4609–4616

more accessible by the M101A mutation. Why M101A encourages the dead-end complex is unknown, but one possibility is that Met101 influences enzyme dynamics in the final step of the mechanism (step 6, Figure 2). Step 6 involves an orchestrated sequence of events involving motion of $NADP^+$, FAD, and the Tyr loop. The structures of the wild-type enzyme complexed with $NADP^+$ reveal steric blocks that must be resolved for the enzyme to return to the resting state. The structures suggest that $NADP^+$ must dissociate first to allow enough room for the FAD to rotate around its C1′−C2′ and N10−C1′ bonds into the *out* conformation. Finally, the Tyr loop moves to cover the *re*-face of the *out* FAD, as shown in Figure 3 (yellow). Apparently, Met101 plays a role in this sequence of molecular motions. We note that Met101 adopts two different side chain conformations in SidA structures, including dual conformations in the $NADP^+$ complex (Figure 5B, aquamarine), which indicates that Met101 is flexible. Our work suggests that this flexibility may have a purpose in resetting the enzyme to its resting state. Another possibility is that Met101 helps stabilize the *in* conformation by acting as a guide that facilitates hydrogen bonding of the pyrimidine edge of the isoalloxazine (Figure 3). Without Met101, the FAD may be more prone to slipping into the *out* state prior to the release of $NADP^+$, resulting in the dead-end state observed *in crystallo*. In this scenario, Met101 may help control the order of protein and flavin motions that are needed for proper product release and resetting the enzyme for the next round of catalysis.

■ ASSOCIATED CONTENT

Supporting Information

The Supporting Information is available free of charge at https://pubs.acs.org/doi/10.1021/acs.biochem.0c00783.

Table S1 and Figures S1−S7 (PDF)

Accession Codes

SidA protein, E9QYP0 (UniProt); SidA M101A resting state, 7JVK (PDB); SidA M101A complexed with $NADP^+$, 7JVL (PDB).

■ AUTHOR INFORMATION

Corresponding Authors

Pablo Sobrado − *Department of Biochemistry and Center for Drug Discovery, Virginia Tech, Blacksburg, Virginia 24061, United States;* orcid.org/0000-0003-1494-5382; Email: psobrado@vt.edu

John J. Tanner − *Department of Biochemistry and Department of Chemistry, University of Missouri, Columbia, Missouri 65211, United States;* orcid.org/0000-0001-8314-113X; Email: tannerjj@missouri.edu

Authors

Ashley C. Campbell − *Department of Biochemistry, University of Missouri, Columbia, Missouri 65211, United States;* orcid.org/0000-0002-0178-4017

Reeder Robinson − *Department of Biochemistry and Center for Drug Discovery, Virginia Tech, Blacksburg, Virginia 24061, United States*

Didier Mena-Aguilar − *Department of Biochemistry and Center for Drug Discovery, Virginia Tech, Blacksburg, Virginia 24061, United States*

Complete contact information is available at: https://pubs.acs.org/10.1021/acs.biochem.0c00783

Author Contributions

A.C.C. performed X-ray diffraction experiments and structure refinement. D.M.-A. performed protein purification. R.R. performed site-directed mutagenesis and kinetic studies. A.C.C. and D.M.-A. performed crystallization. J.J.T. and P.S. wrote the initial draft of the manuscript. All authors analyzed data and reviewed the final version of the manuscript.

Funding

This research was supported by National Science Foundation Grants CHE-2003658 (to P.S.) and CHE-2003986 (to J.J.T.).

Notes

The authors declare no competing financial interest.

■ ACKNOWLEDGMENTS

The authors thank Hannah Valentino for help with data analysis and J. Nix for help with remote X-ray diffraction data collection at beamline 4.2.2. Beamline 4.2.2 of the Advanced Light Source, a U.S. Department of Energy Office of Science User Facility under Contract DE-AC02-05CH11231, is supported in part by the ALS-ENABLE program funded by the National Institutes of Health, National Institute of General Medical Sciences, Grant P30 GM124169-01.

■ ABBREVIATIONS

L-Orn, L-ornithine; SidA, siderophore biosynthetic enzyme A; NMO, N-hydroxylating flavin-dependent monooxygenase; PDB, Protein Data Bank; SKIE, solvent kinetic isotope effect.

■ REFERENCES

(1) Hissen, A. H., Wan, A. N., Warwas, M. L., Pinto, L. J., and Moore, M. M. (2005) The Aspergillus fumigatus siderophore biosynthetic gene sidA, encoding L-ornithine N5-oxygenase, is required for virulence. *Infect. Immun. 73*, 5493−5503.

(2) Chocklett, S. W., and Sobrado, P. (2010) Aspergillus fumigatus SidA is a highly specific ornithine hydroxylase with bound flavin cofactor. *Biochemistry 49*, 6777−6783.

(3) Martín Del Campo, J. S., Vogelaar, N., Tolani, K., Kizjakina, K., Harich, K., and Sobrado, P. (2016) Inhibition of the Flavin-Dependent Monooxygenase Siderophore A (SidA) Blocks Siderophore Biosynthesis and Aspergillus fumigatus Growth. *ACS Chem. Biol. 11*, 3035−3042.

(4) Romero, E., Fedkenheuer, M., Chocklett, S. W., Qi, J., Oppenheimer, M., and Sobrado, P. (2012) Dual role of NADP(H) in the reaction of a flavin dependent N-hydroxylating monooxygenase. *Biochim. Biophys. Acta, Proteins Proteomics 1824*, 850−857.

(5) Haas, H. (2014) Fungal siderophore metabolism with a focus on Aspergillus fumigatus. *Nat. Prod. Rep. 31*, 1266−1276.

(6) Palfey, B. A., and McDonald, C. A. (2010) Control of catalysis in flavin-dependent monooxygenases. *Arch. Biochem. Biophys. 493*, 26−36.

(7) Campbell, A. C., Stiers, K. M., Martin Del Campo, J. S., Mehra-Chaudhary, R., Sobrado, P., and Tanner, J. J. (2020) Trapping conformational states of a flavin-dependent N-monooxygenase in crystallo reveals protein and flavin dynamics. *J. Biol. Chem. 295*, 13239−13249.

(8) Setser, J. W., Heemstra, J. R., Jr., Walsh, C. T., and Drennan, C. L. (2014) Crystallographic evidence of drastic conformational changes in the active site of a flavin-dependent N-hydroxylase. *Biochemistry 53*, 6063−6077.

(9) Robinson, R., Badieyan, S., and Sobrado, P. (2013) C4a-hydroperoxyflavin formation in N-hydroxylating flavin monooxygenases is mediated by the 2′-OH of the nicotinamide ribose of NADP(+). *Biochemistry 52*, 9089−9091.

(10) Franceschini, S., Fedkenheuer, M., Vogelaar, N. J., Robinson, H. H., Sobrado, P., and Mattevi, A. (2012) Structural insight into the

mechanism of oxygen activation and substrate selectivity of flavin-dependent N-hydroxylating monooxygenases. *Biochemistry 51*, 7043−7045.
(11) Crooks, G. E., Hon, G., Chandonia, J. M., and Brenner, S. E. (2004) Web Logo: a sequence logo generator. *Genome Res. 14*, 1188−1190.
(12) Chocklett, S. W., and Sobrado, P. (2010) Aspergillus fumigatus SidA Is a Highly Specific Ornithine Hydroxylase with Bound Flavin Cofactor. *Biochemistry 49*, 6777−6783.
(13) Csaky, T. Z., Hassel, O., Rosenberg, T., Lang, S., Turunen, E., and Tuhkanen, A. (1948) On the estimation of bound hydroxylamine in biological materials. *Acta Chem. Scand. 2*, 450−454.
(14) Schowen, K. B., and Schowen, R. L. (1982) Solvent isotope effects of enzyme systems. *Methods Enzymol. 87*, 551−606.
(15) Kabsch, W. (2010) XDS. *Acta Crystallogr., Sect. D: Biol. Crystallogr. 66*, 125−132.
(16) Evans, P. R., and Murshudov, G. N. (2013) How good are my data and what is the resolution? *Acta Crystallogr., Sect. D: Biol. Crystallogr. 69*, 1204−1214.
(17) Luo, M., Gamage, T. T., Arentson, B. W., Schlasner, K. N., Becker, D. F., and Tanner, J. J. (2016) Structures of Proline Utilization A (PutA) Reveal the Fold and Functions of the Aldehyde Dehydrogenase Superfamily Domain of Unknown Function. *J. Biol. Chem. 291*, 24065−24075.
(18) Afonine, P. V., Grosse-Kunstleve, R. W., Echols, N., Headd, J. J., Moriarty, N. W., Mustyakimov, M., Terwilliger, T. C., Urzhumtsev, A., Zwart, P. H., and Adams, P. D. (2012) Towards automated crystallographic structure refinement with phenix.refine. *Acta Crystallogr., Sect. D: Biol. Crystallogr. 68*, 352−367.
(19) Emsley, P., Lohkamp, B., Scott, W. G., and Cowtan, K. (2010) Features and development of Coot. *Acta Crystallogr., Sect. D: Biol. Crystallogr. 66*, 486−501.
(20) Chen, V. B., Arendall, W. B., 3rd, Headd, J. J., Keedy, D. A., Immormino, R. M., Kapral, G. J., Murray, L. W., Richardson, J. S., and Richardson, D. C. (2010) Mol Probity: all-atom structure validation for macromolecular crystallography. *Acta Crystallogr., Sect. D: Biol. Crystallogr. D66*, 12−21.
(21) Gore, S., Sanz Garcia, E., Hendrickx, P. M. S., Gutmanas, A., Westbrook, J. D., Yang, H., Feng, Z., Baskaran, K., Berrisford, J. M., Hudson, B. P., Ikegawa, Y., Kobayashi, N., Lawson, C. L., Mading, S., Mak, L., Mukhopadhyay, A., Oldfield, T. J., Patwardhan, A., Peisach, E., Sahni, G., Sekharan, M. R., Sen, S., Shao, C., Smart, O. S., Ulrich, E. L., Yamashita, R., Quesada, M., Young, J. Y., Nakamura, H., Markley, J. L., Berman, H. M., Burley, S. K., Velankar, S., and Kleywegt, G. J. (2017) Validation of Structures in the Protein Data Bank. *Structure 25*, 1916−1927.
(22) Liebschner, D., Afonine, P. V., Moriarty, N. W., Poon, B. K., Sobolev, O. V., Terwilliger, T. C., and Adams, P. D. (2017) Polder maps: improving OMIT maps by excluding bulk solvent. *Acta Crystallogr. D Struct Biol. 73*, 148−157.
(23) Romero, E., Fedkenheuer, M., Chocklett, S. W., Qi, J., Oppenheimer, M., and Sobrado, P. (2012) Dual role of NADP(H) in the reaction of a flavin dependent N-hydroxylating monooxygenase. *Biochim. Biophys. Acta, Proteins Proteomics 1824*, 850−857.
(24) Robinson, R. M., Klancher, C. A., Rodriguez, P. J., and Sobrado, P. (2019) Flavin oxidation in flavin-dependent N-monooxygenases. *Protein Sci. 28*, 90−99.
(25) Huijbers, M. M., Montersino, S., Westphal, A. H., Tischler, D., and van Berkel, W. J. (2014) Flavin dependent monooxygenases. *Arch. Biochem. Biophys. 544*, 2−17.
(26) Ballou, D. P., Entsch, B., and Cole, L. J. (2005) Dynamics involved in catalysis by single-component and two-component flavin-dependent aromatic hydroxylases. *Biochem. Biophys. Res. Commun. 338*, 590−598.
(27) Olucha, J., Meneely, K. M., Chilton, A. S., and Lamb, A. L. (2011) Two structures of an N-hydroxylating flavoprotein monooxygenase: ornithine hydroxylase from Pseudomonas aeruginosa. *J. Biol. Chem. 286*, 31789−31798.
(28) Shirey, C., Badieyan, S., and Sobrado, P. (2013) Role of Ser-257 in the sliding mechanism of NADP(H) in the reaction catalyzed by the Aspergillus fumigatus flavin-dependent ornithine N5-monooxygenase SidA. *J. Biol. Chem. 288*, 32440−32448.
(29) Badieyan, S., Bach, R. D., and Sobrado, P. (2015) Mechanism of N-hydroxylation catalyzed by flavin-dependent monooxygenases. *J. Org. Chem. 80*, 2139−2147.

https://dx.doi.org/10.1021/acs.biochem.0c00783
Biochemistry 2020, 59, 4609−4616